






## Open Archive Toulouse Archive Ouverte

OATAO is an open access repository that collects the work of Toulouse researchers and makes it freely available over the web where possible

This is an author's version published in: <http://oatao.univ-toulouse.fr/20794>

### To cite this version:

Zami-Pierre, Frédéric  and Loubens, Romain de and Quintard, Michel  and Davit, Yohan  *Effect of disorder in the pore-scale structure on the flow of shear-thinning fluids through porous media*. (2018) *Journal of Non-Newtonian Fluid Mechanics*, 261. 99-110. ISSN 0377-0257

Any correspondence concerning this service should be sent  
to the repository administrator: [tech-oatao@listes-diff.inp-toulouse.fr](mailto:tech-oatao@listes-diff.inp-toulouse.fr)

# Effect of disorder in the pore-scale structure on the flow of shear-thinning fluids through porous media

F. Zami-Pierre<sup>a,b</sup>, R. de Loubens<sup>b</sup>, M. Quintard<sup>a</sup>, Y. Davit<sup>a,b,\*</sup>

<sup>a</sup> *Institut de Mécanique des Fluides de Toulouse (IMFT), Université de Toulouse, CNRS, INPT, UPS, Toulouse, France*

<sup>b</sup> *Total, CSTJF, Avenue Larribau, Pau 64018, France*

---

## A B S T R A C T

Modeling the flow of fluids with shear-dependent viscosity through porous media is a challenging fundamental and engineering problem. At continuum-scale, such flows are usually described using modified versions of Darcy's law, which are obtained by considering either an apparent viscosity or an apparent permeability. In the two cases, Darcy's law becomes nonlinear as the apparent viscosity or permeability both depend on the velocity or pressure gradient. The main difference between these two approaches is the impact of non-Newtonian effects on the flow direction. With the apparent viscosity, the flow direction is determined by the standard permeability tensor and unaltered by non-Newtonian effects. On the other hand, with the apparent permeability, the flow direction may be modified by non-Newtonian effects contained in the second-order tensor. Here, we ask the question of whether it is necessary to use a general tensorial correction including changes of flow direction or if the (scalar) apparent viscosity approach is sufficient. To study this, we solve numerically the non-Newtonian flow problem in a variety of isotropic porous structures for a model fluid where the viscosity depends on the shear rate following a power law with a Newtonian cut-off in the limit of low shear rates. We find that the structure of the porous medium plays a fundamental role and that there is a competition between the nonlinearity of the flow, induced by the non-Newtonian rheology, and the disorder of the porous structure. Our main result is that an apparent viscosity is sufficient in cases of sufficiently disordered porous media, as is the case of some sandstones found in petroleum engineering. Fundamentally, this suggests that the disorder in the geometry of the porous structure is mitigating part of the nonlinear effects due to the rheology.

---

## 1. Introduction

Many aspects of the fundamental physics of non-Newtonian flows through porous media, as found in practical applications ranging from composites manufacturing [1] to blood flow in the vascular system [2,3] or Enhanced Oil Recovery (EOR) [4], are still poorly understood. Nonlinear effects, such as those associated with yield stress or Bingham fluids [5], shear-dependent viscosity [6] or viscoelastic fluids [7], make flow through porous media very complex and the development of continuum scale models challenging. In this work, we consider the flow of a model shear-thinning fluid, belonging to the class of Bird–Carreau fluids [6], that is Newtonian in the limit of low shear rates and shear-thinning for larger values. The flow of such fluids through porous media is often modelled by a modified Darcy's law with an apparent viscosity [4,8–10],

$$\langle \mathbf{v} \rangle = - \frac{K_0}{\mu_{\text{app}}(\langle \mathbf{v} \rangle)} \cdot (\nabla \langle p \rangle^\beta - \rho \mathbf{g}), \quad (1)$$

with  $K_0$  the intrinsic, or standard, permeability,  $\langle \mathbf{v} \rangle$  the average superficial velocity,  $\nabla \langle p \rangle^\beta$  the pressure gradient (where  $\langle p \rangle^\beta$  is the intrinsic average pressure) and  $\rho \mathbf{g}$  the gravity term.  $\mu_{\text{app}}(\langle \mathbf{v} \rangle)$  is the apparent viscosity that is used to capture the influence of non-Newtonian effects and is often considered a function of the velocity, therefore yielding a nonlinear form of Darcy's law. If the fluid is Newtonian, the apparent viscosity  $\mu_{\text{app}}$  simply reduces to a constant viscosity,  $\mu_0$ , and the classic Darcy's law is recovered.

In the context of polymer solutions used in petroleum engineering, the use of such an apparent viscosity dates back to the sixties, see for instance [11] or [12]. To estimate this apparent viscosity, [9] latter introduced the concept of an apparent shear rate that is used to calculate the apparent viscosity directly from the expression of the shear-dependent viscosity of the bulk fluid and the average velocity. Although ubiquitous in engineering and useful in practical cases, the limitations of this approach, which is essentially based on analytical solutions in the case of capillary tubes, are not evident. One of the main issues of the concept

of apparent viscosity is that it inherently assumes that non-Newtonian effects do not affect the orientation of the flow. Indeed, we note in Eq. (1) that the vectors  $\langle \mathbf{v} \rangle$  and  $\mathbf{K}_0 \cdot (\nabla \langle p \rangle^\beta - \rho \mathbf{g})$  are necessarily colinear. There is no particular reason for this to be always correct. In fact, several studies have even shown that the direction of  $\langle \mathbf{v} \rangle$  and  $\mathbf{K}_0 \cdot (\nabla \langle p \rangle^\beta - \rho \mathbf{g})$  may actually be different in the case of a non-Newtonian fluid flow [13–15].

One way to circumvent this problem is to define a second-order apparent permeability tensor, noted  $\mathbf{K}_{\text{app}}$ , and decompose it into a scalar  $k_n$  and a rotation matrix  $\mathbf{P}$ . Within this framework, Eq. (1) is replaced by

$$\langle \mathbf{v} \rangle = -\frac{\mathbf{K}_{\text{app}}}{\mu_0} \cdot (\nabla \langle p \rangle^\beta - \rho \mathbf{g}), \quad (2)$$

where  $\mu_0$  is an *arbitrary* reference viscosity (for instance the viscosity in the limit of very low shear rates for polymer solutions) and  $\mathbf{K}_{\text{app}} = k_n \mathbf{P} \cdot \mathbf{K}_0$ . This formulation is more general as it includes the case of the apparent viscosity ( $\mathbf{P} = \mathbf{I}$  and  $k_n = \mu_0/\mu_{\text{app}}$ ) and can also capture cases where the vectors  $\langle \mathbf{v} \rangle$  and  $\mathbf{K}_0 \cdot (\nabla \langle p \rangle^\beta - \rho \mathbf{g})$  have different directions ( $\mathbf{P} \neq \mathbf{I}$ , anisotropy induced by the non-linear viscosity).

Our strategy in this work consists in using numerical simulations of the flow of PLCO fluids at the pore scale over a broad range of porous structures, as detailed in Section 2, to study the behavior of  $k_n \mathbf{P}$  in Section 3. More specifically, we wish to answer the following questions: What are the values of  $k_n$  and  $\mathbf{P}$  in the different flow regimes? What is the effect of disorder in the porous structure on  $k_n \mathbf{P}$ ? Is it ever correct to use only a scalar in Darcy's law to represent the non-Newtonian effects? In addition to these fundamental questions, a discussion specific to reservoir simulator models used for the flow of polymer solutions in EOR (Enhanced Oil Recovery) is provided in Section 4.2.

## 2. Models and methods

### 2.1. The pore-scale flow model

In this section, we describe the flow model, limiting our study to the steady, incompressible, single-phase, creeping flow of a liquid ( $\beta$ -phase) through a rigid porous medium ( $\sigma$ -phase). Momentum and mass balance equations read

$$\nabla \cdot [\mu(\dot{\gamma})(\nabla \mathbf{v} + (\nabla \mathbf{v})^T)] - \nabla p + \rho \mathbf{f} = 0 \text{ in } V_\beta, \quad (3)$$

$$\nabla \cdot \mathbf{v} = 0 \text{ in } V_\beta, \quad (4)$$

where  $\rho \mathbf{f}$  is a volume force,  $\mathbf{v}$  the velocity field and  $p$  the pressure field. Here, the non-Newtonian rheology is captured by  $\mu(\dot{\gamma})$ , see Section 2.2, with  $\dot{\gamma}$  the local shear rate, and is the only source of nonlinearity in the problem. For the solid/liquid interface, we consider the simple no-slip condition,

$$\mathbf{v} = 0 \text{ at } A_{\beta\sigma}, \quad (5)$$

therefore neglecting specific effects, such as rearrangements of polymer chains near the wall in the case of polymer solutions, that can often be described using an effective slip boundary condition [16].

### 2.2. The rheology

Many complex fluids are shear-thinning/thickening and feature cut-off effects depending on the local shear rate or local stress. This is the case of polymer solutions, which have the ability to strongly modify the rheological response of the bulk fluid, even at low concentrations. Dilute or semi-dilute solutions of partially hydrolyzed polyacrylamides (HPAM) and xanthan polymers, which are used in practical EOR situations [4], are known to be shear-thinning. Further, they often behave as Newtonian fluids in the limit of very low shear rates and reach a shear-thinning limit at very large shear rates. To represent these phenomena,

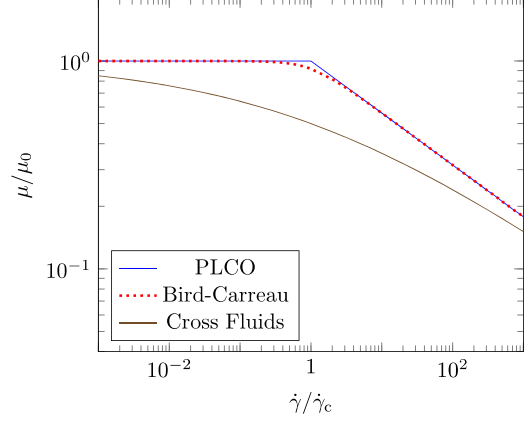


Fig. 1. Evolution of the normalized shear viscosity ( $\mu/\mu_0$ ) as a function of the normalized shear rate ( $\dot{\gamma}/\dot{\gamma}_c$ ) in log-log scale for the power-law with cut-off (PLCO), Bird-Carreau and cross fluids models.

several models are available, see Fig. 1. The most common model is probably the Bird–Carreau [6].

In this study, we consider a model fluid with a power-law with cut-off (PLCO) rheology,

$$\mu(\dot{\gamma}) = \begin{cases} \mu_0 & \text{if } \dot{\gamma} < \dot{\gamma}_c, \\ \mu_0 \left( \frac{\dot{\gamma}}{\dot{\gamma}_c} \right)^{n-1} & \text{otherwise,} \end{cases} \quad (6)$$

where  $\dot{\gamma}_c$  is a critical shear rate and  $n$  is the parameter that controls the non-linearity ( $n = 1$  corresponds to the Newtonian rheology). The focal feature of this law is that it captures both the Newtonian asymptote at low shear rates and the power-law shear-thinning behavior at high shear rates. The rationale for using this model is twofold. First, this is one of the simplest models that captures these two effects, therefore allowing us to understand fundamental aspects of such flows with a minimal number of parameters. More sophisticated models [6] may slightly affect the transition regime but do not modify the main results presented in this paper. Second, there are complex fluids, such as polymer solutions, for which the PLCO remains a reasonable description, especially for xanthan, a semi-rigid rod-like polymer [17]. For simplicity, we use  $\dot{\gamma}_c = 1 \text{ s}^{-1}$  and  $\mu_0 = 3.5 \text{ cP}$  (which is consistent with dilute solutions of xanthan) in the remainder of the paper. Our results do not depend on these specific values, which act only as scaling parameters. Moreover, the proposed methodology is not limited to PLCO model. The theory and implemented numerical models can be readily applied to different rheological behaviors. For Bird-Carreau and Cross fluids, this would essentially have a quantitative impact, without modifications of the fundamental conclusions.

### 2.3. The macroscale flow model

One way to connect the pore-scale physics with the continuum models is to use upscaling procedures. These are generally used to derive macroscale laws directly from the fundamental principles at the pore scale. A variety of approaches exist (see discussions in [18]), including the volume averaging method (VAM) or homogenization [19]. For instance, Whitaker in [20] showed that for the creeping incompressible flow of a Newtonian fluid with a no-slip condition at the solid/liquid interface, the classical Darcy's law is obtained [21],

$$\langle \mathbf{v} \rangle = -\frac{\mathbf{K}_0}{\mu_0} \cdot (\nabla \langle p \rangle^\beta - \rho \mathbf{g}). \quad (7)$$

One of the main results of the VAM is that the intrinsic permeability  $\mathbf{K}_0$  is a function of closure variables and can be calculated for a given porous structure (see Appendix B for an introduction to the concept of

closure) independently from the viscosity. For linear flows, the link between the pore-scale physics and the continuum-scale models is now well understood. However, the same is not true of non-Newtonian flows that are described by non-linear partial differential equations, for which upscaling is a lot more difficult and requires additional assumptions. Appendix B illustrates the shortcomings of a procedure based on the standard volume averaging method (see [20]) applied to a generic non-Newtonian fluid. There are few very specific cases for which upscaling approaches have been used, such as the case of a pure power-law rheological model ( $\mu \propto \dot{\gamma}^{n-1}$ ) [13,15] for which many theoretical analysis and numerical studies have shown that the permeability is proportional to  $\|\langle \mathbf{v} \rangle\|^{1-n}$  [14,22]. These results are also largely validated by data collected from coreflood experiments [9,23,24]. However, these studies are limited to a pure power-law fluid, which fail to capture regime transitions, and to simple unit-cell geometries.

Here, we postulate that the macroscale flow can be described by the generalized Darcy's law (see Appendix B),

$$\langle \mathbf{v} \rangle = -\frac{K_{\text{app}}}{\mu_0} \cdot (\nabla \langle p \rangle^\beta - \rho \mathbf{g}). \quad (8)$$

To further account for changes in the flow direction between the Newtonian and non-Newtonian regimes, we write

$$K_{\text{app}} = k_n \mathbf{P} \cdot K_0, \quad (9)$$

with the scalar,  $k_n$ , capturing a change in the velocity norm due to non-Newtonian effects and the rotation tensor  $\mathbf{P}$  capturing changes in the direction of the average velocity [13–15]. The rotation tensor  $\mathbf{P}$  may be written as

$$\mathbf{P} = \begin{bmatrix} 1 & 0 & 0 \\ 0 & \cos(\gamma) & -\sin(\gamma) \\ 0 & \sin(\gamma) & \cos(\gamma) \end{bmatrix} \cdot \begin{bmatrix} \cos(\alpha) & -\sin(\alpha) & 0 \\ \sin(\alpha) & \cos(\alpha) & 0 \\ 0 & 0 & 1 \end{bmatrix}, \quad (10)$$

with  $\alpha$  and  $\gamma$  the rotation angles. We note that:

1. if the nonlinearity does not affect the average velocity direction, then  $\mathbf{P} = \mathbf{I}$ ;
2. in a general nonlinear case, both  $k_n$  and  $\mathbf{P}$  are *a priori* functions of  $\langle \mathbf{v} \rangle$  (module and orientation);
3. and while in the linear case the permeability tensor  $K_0$  is symmetric, the same is not true of  $K_{\text{app}}$  because of nonlinear effects [25].

The macroscopic model is therefore

$$\langle \mathbf{v} \rangle = -k_n \mathbf{P} \cdot \frac{K_0}{\mu_0} \cdot (\nabla \langle p \rangle^\beta - \rho \mathbf{g}) = k_n \mathbf{P} \cdot \langle \mathbf{v}_0 \rangle, \quad (11)$$

with  $\langle \mathbf{v}_0 \rangle$  the average velocity associated with the linear flow regime at the same value of  $\nabla \langle p \rangle^\beta - \rho \mathbf{g}$ . When the fluid is Newtonian, the velocity resulting from the source term  $\nabla \langle p \rangle^\beta - \rho \mathbf{g}$  is called hereafter the *Newtonian average velocity* and is noted  $\langle \mathbf{v}_0 \rangle$ . When the fluid is non-Newtonian, the velocity resulting from the same source term  $\nabla \langle p \rangle^\beta - \rho \mathbf{g}$  is called the *non-Newtonian average velocity* and is noted  $\langle \mathbf{v} \rangle$ .

#### 2.4. The porous structures

To understand the role of  $k_n \mathbf{P}$  in Eq. (11), we are going to solve numerically the flow problem at the pore scale over a variety of porous structures. All these structures are treated as locally periodic, so that effective properties  $K_0$ ,  $k_n$  and  $\mathbf{P}$  can be easily calculated by pore-scale simulations with periodic conditions applied to  $\mathbf{v}$  and  $p$  (the reader is referred to [26] for a discussion on how to apply periodic conditions to tomographic images of intrinsically non-periodic media such as natural porous rocks).

##### The array of cylinders

The first class of porous structures that we consider are 2D arrays of  $15 \times 15$  cylinders, denoted as A-type (A standing for array), corresponding to an area of  $15 \times 15 \text{ mm}^2$ . Our goal in studying these model porous media is to assess the impact of disorder on the apparent permeability.

These structures are created by first positioning the cylinders on a regular grid (medium  $A^{\sigma=0}$ , see Fig. 2a) and then disturbing their position. To do so, we randomly select one cylinder and displace it with a uniform probability for the direction and a centered Gaussian law for the amplitude with the constraints that 1) periodic boundaries must be preserved and 2) overlapping is prohibited. The amplitude of the displacement is characterized by the standard deviation  $\sigma$  of the Gaussian law, which is used as a proxy to measure disorder [27]. Then, the procedure is repeated for another cylinder randomly selected among the remaining ones until all cylinders have been displaced. This method generates slight biases in the distribution of the cylinder displacements, which is not truly Gaussian because of the constraints described above. For each value of  $\sigma$ , 10 porous media are generated and are denoted by  $A_i^{\sigma \neq 0}$ . Examples of geometries with various degrees of disorder are presented in Fig. 2a–e.

##### The Bentheimer sandstone

The second class of porous structure that we consider is a Bentheimer sandstone, namely B (of volume  $1 \text{ mm}^3$ ), represented in Fig. 2f. This medium is similar to sandstones encountered in EOR applications [28]. The geometry of this medium was extracted from x-ray micro tomography (see discussions about the related problems of the procedure in [29]).

#### 2.5. Setting of numerical simulations

The pore-scale flow problem is solved using the finite volume toolbox OpenFOAM [30] via a SIMPLE algorithm (see e.g. Patankar [31]). Mesh convergence is studied for unstructured hex-dominant meshes that are generated for each medium. For the two-dimensional structures, we could afford to use uniform meshes. However, for the three-dimensional sandstone, we achieved grid convergence by performing local mesh refinements within the pore throats. These pore throats are defined by the distance to the wall (using the tool *close-proximity feature detection* in OpenFOAM). We apply periodic boundary conditions on  $\mathbf{v}$  and  $p$ . For A-type media, this condition is straightforward since these media are spatially periodic by construction. For medium B, this condition is ensured by surrounding the medium with a very thin layer of liquid (of thickness  $0.5 \mu\text{m}$ ) on all sides [32]. This layer was generated as thin as possible in order to avoid preferential flows of fluid around the medium.

To study  $k_n$  and  $\mathbf{P}$  under various flow conditions, we impose a source term  $\rho \mathbf{f}$  in the momentum equation to generate the flow, which plays the role of  $-(\nabla \langle p \rangle^\beta - \rho \mathbf{g})$  in Darcy's law (Eq. (11)). The direction of the source term is specified with radial coordinates as

$$\rho \mathbf{f} = \rho \|\mathbf{f}\| \begin{pmatrix} \cos(\theta) \\ \sin(\theta) \\ 0 \end{pmatrix}. \quad (12)$$

In all the cases presented in this work, the source term is imposed in the plane ( $\mathbf{e}_x, \mathbf{e}_y$ ). Fig. 3 illustrates in two dimensions the source vector  $\rho \mathbf{f}$  and the associated Newtonian,  $\langle \mathbf{v}_0 \rangle$ , and non-Newtonian,  $\langle \mathbf{v} \rangle$ , average velocities. In two dimensions, only the angle  $\alpha$  is needed in the rotation matrix  $\mathbf{P}$  (see Eq. (10)).

#### 2.6. Metrics and statistics

To investigate the macroscale behavior with various degrees of disorder, the dimensionless intrinsic permeability  $K_0^*$  is defined for the A-type media as

$$K_0^* = \frac{K_0}{\|K_0^{\sigma=0}\|}, \quad (13)$$

with  $K_0^{\sigma=0}$  the permeability of medium  $A^{\sigma=0}$ . Following the same idea, the parameter  $k_n^*$  is defined as

$$k_n^* = \frac{k_n}{k_n^{\sigma=0}}. \quad (14)$$



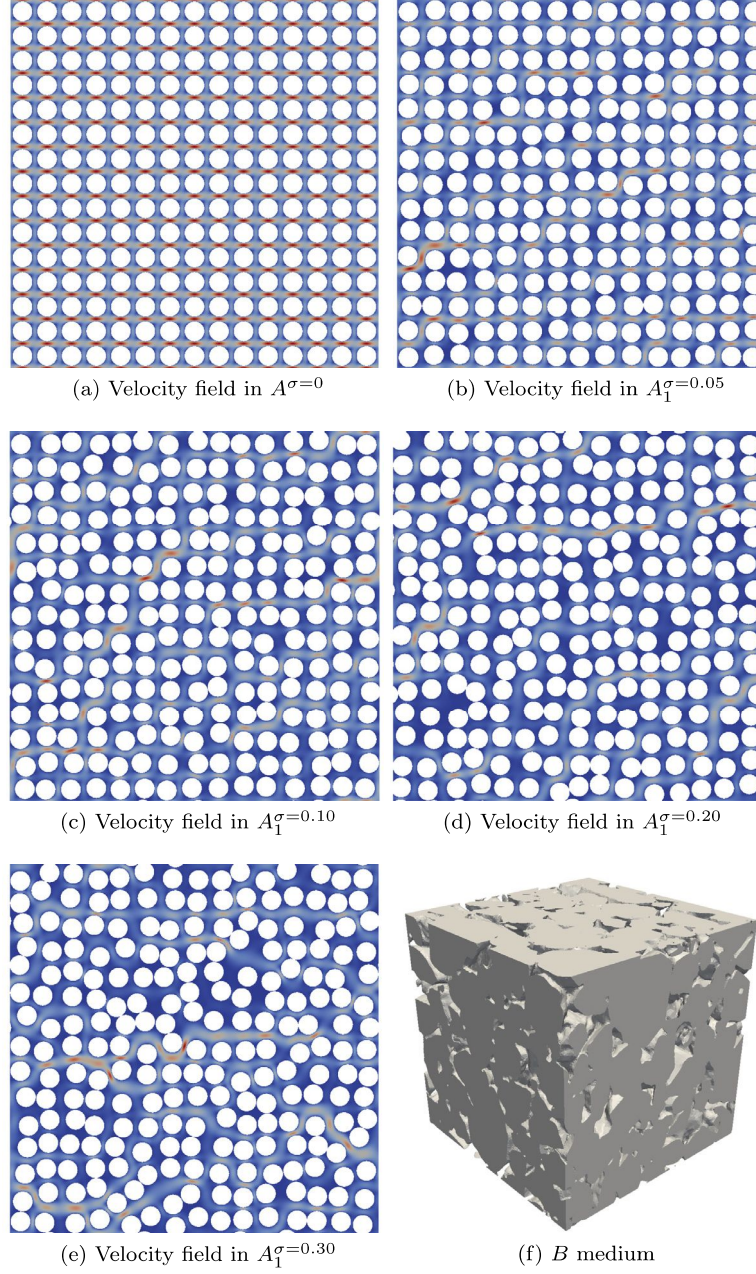


**Fig. 2.** Porous structures investigated in this study. (a)–(e): velocity fields of a Newtonian flow imposed in the array of cylinders (denoted A-type, area of  $15 \times 15 \text{ mm}^2$ ) with various degrees of disorder and a source term  $\rho f$  imposed with  $\theta = 22.5^\circ$  (see Eq. (12)). (f): solid phase of the Bentheimer sandstone B (of volume  $1 \text{ mm}^3$ ).

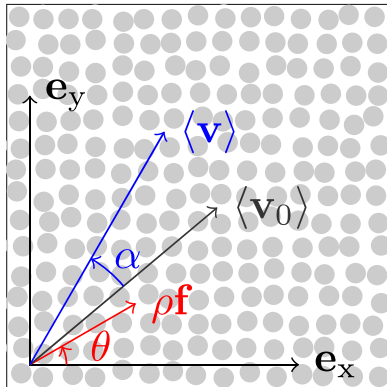


**Fig. 3.** Angles used in a 2D case.

To further investigate the statistics of the results, we define the expected value  $E(\psi)$  for each macroscale variable  $\psi$  as the average of  $\psi$  over the 10 realizations corresponding to each value of  $\sigma$ . The standard deviation,

$$\Sigma(\psi) = \sqrt{E(\psi^2) - E(\psi)^2}, \quad (15)$$

is also calculated for each value of  $\sigma$ . Using the A-type media, we investigate the macroscale behavior in the linear case (via the parameter  $\|K_0^*\|$ ) and in the nonlinear case (via the parameters  $k_n$ ,  $\alpha$  and  $\gamma$ , see Eq. (9)) as a function of the disorder.

For several Figures of this paper (4, 5 and 7), the same statistical representation is used for the A-type media. For a macroscale variable  $\psi$ , the average  $E(\psi)$  is represented by (red) disks. The standard deviation  $\Sigma(\psi)$  is represented by error bars (the lower and higher tips of the bars represent respectively  $E(\psi) - \Sigma(\psi)$  and  $E(\psi) + \Sigma(\psi)$ ). Finally, the (blue) circles represent the minimum and maximum values of  $\psi$ .

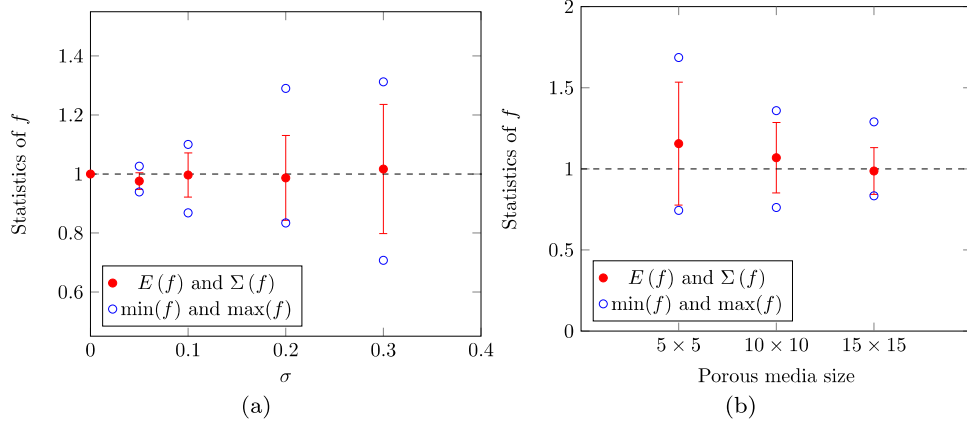


**Fig. 4.** Statistics of the anisotropy factor  $f$  for the A-type media. (a) evolution with the disorder, characterized by  $\sigma$  and (b) evolution with the porous medium size for  $\sigma = 0.20$  ( $5 \times 5$ ,  $10 \times 10$  and  $15 \times 15$  cylinders).

## 2.7. Statistical isotropy of A-type media

To ensure that the process used to generate the A-type media is correct, we check here that the disordered media are isotropic. To estimate the degree of anisotropy, we calculate the so-called permeability anisotropy factor  $f$  with the two eigenvalues  $d_{xx}$  and  $d_{yy}$  of  $K_0$ ,

$$f = \frac{d_{xx}}{d_{yy}}. \quad (16)$$

For each realization and each value of  $\sigma$ , we therefore calculate the full intrinsic permeability tensor  $K_0$  and then the anisotropy factor  $f$ , see Eq. (16).

Fig. 4a shows that, as the disorder increases, the average value of the anisotropy factor  $E(f)$  remains close to unity. The minimum and maximum values of  $f$  are also close to unity (the largest deviation is observed for  $\sigma = 0.3$  where the minimum and maximum values of  $f$  are respectively close to 0.70 and 1.30). Despite the fact that each realization is not isotropic, Fig. 4a allows us to consider the ensemble as statistically isotropic since the expected value of  $f$  for only 10 realizations is very close to 1.

We also observe in Fig. 4a that, for a given size of the domain,  $\Sigma(f)$  increases with  $\sigma$ . We hypothesize that this is due to the finite size of the considered domain, which may not be large enough to ensure isotropy and statistical convergence when  $\sigma$  is large. For instance, we clearly see in Figs. 2a to 2e that increasing  $\sigma$  leads to structures with characteristic lengthscales (aggregates of cylinders and preferential flow paths) much larger than the cylinder diameter. Further, given the procedure for generating these disordered structures and the periodic conditions, we expect some form of ergodicity between ensemble and spatial averages. Fig. 4b, which shows that the variance of ensemble averaging strongly decreases with the size of the domain, confirms this ergodicity. Ergodicity is also proven using a domain of size  $50 \times 50$  cylinders, see Appendix A. For a domain size of  $15 \times 15$ , which is the size used in the remainder of the paper, we can consider only 10 realizations to obtain statistically converged results for  $f$ . Following the same idea, we verified that the results were statistically converged for the nonlinear parameters  $k_n$  and  $P$ , even though the results are not presented.

## 3. Results

To better understand how nonlinear effects develop and how they affect the macroscale transport properties, this section starts with a description of the Newtonian case, then moves on to study the transition regime and finally describes the fully non-Newtonian regime. In particular, we will see that this allows us to characterize the non-Newtonian regime and clearly define the domains of validity of our interpretations.

**Table 1**

Characteristics (porosity, permeability and anisotropy factor) of the porous media investigated. The permeability  $K_0$  is expressed in  $\mu\text{m}^2$ . The anisotropy factor  $f$  is defined in Eq. (16).

Medium	$\phi$	$K_0$	$f$
$A^{\sigma=0}$	0.4973	$\begin{pmatrix} 1828 & 0 \\ 0 & 1828 \end{pmatrix}$	1
$A_1^{\sigma=0.05}$	0.4973	$\begin{pmatrix} 1817 & 57 \\ 57 & 1812 \end{pmatrix}$	0.94
$A_1^{\sigma=0.1}$	0.4950	$\begin{pmatrix} 1743 & 70 \\ 70 & 1827 \end{pmatrix}$	1.09
$A_1^{\sigma=0.2}$	0.4950	$\begin{pmatrix} 1672 & 151 \\ 151 & 1671 \end{pmatrix}$	0.83
$A_1^{\sigma=0.3}$	0.4950	$\begin{pmatrix} 1626 & 37 \\ 37 & 1380 \end{pmatrix}$	0.84
$B$	0.25	$\begin{pmatrix} 3.85 & 0.14 & 0.23 \\ 0.14 & 4.32 & 0.22 \\ 0.23 & 0.22 & 4.30 \end{pmatrix}$	0.91

### 3.1. Newtonian flows

We first focus on the Newtonian behavior of the different porous structures presented in Fig. 2. To evaluate differences between these structures, we characterize all media by their porosity  $\phi$ , their intrinsic permeability  $K_0$  and their anisotropy factor  $f$  (see Eq. (16)). Example results are described in Table 1. The calculated values of  $K_0$  for medium  $A^{\sigma=0}$ , which has been intensively investigated in porous media sciences [14,15], is in good agreement with the literature. Further, the value of the permeability for medium  $B$  is also correct for a typical sandstone [33,34]. Regarding isotropy, we find that the media  $A$  are statistically isotropic (see Fig. 4a) and that  $B$  is approximately isotropic.

For disordered structures,  $A^{\sigma \neq 0}$ , Fig. 5 shows the statistical behavior of  $\|K_0^*\|$  with the disorder, as characterized by  $\sigma$ . We observe that  $\Sigma(\|K_0^*\|)$  increases with  $\sigma$ . As discussed above, this is related to the fact that the size of the considered domain may not be large enough to be considered as a representative elementary volume (REV). We also see that  $E(\|K_0^*\|)$  decreases with  $\sigma$ , which we hypothesize is due to the fact that the tortuosity increases with the disorder (see Figs. 2a to 2e).

### 3.2. Transition from Newtonian to non-Newtonian flows

We now investigate the behavior of  $k_n P$  during the transition from a constant to a power-law viscosity. For Newtonian flow at relatively slow velocities, we have that  $k_n P = I$ . For larger values of the velocity, nonlinear effects start to become predominant at the pore scale, leading to changes in  $k_n P$ . To capture this transition, we use the dimensionless

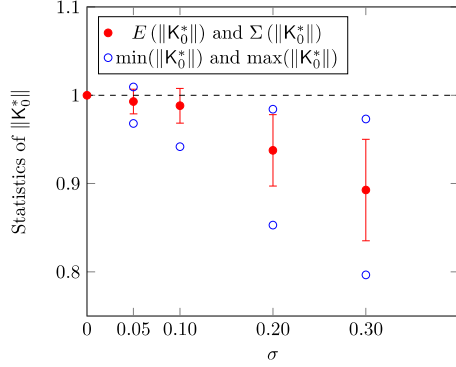


Fig. 5. Statistics of  $\|K_0\|$  for increasing disorder,  $\sigma$ , for the A-type media.

velocity

$$U^* = \frac{\|\langle \mathbf{v} \rangle\|}{\phi \dot{\gamma}_c \sqrt{\|K_0\|}}, \quad (17)$$

with  $\|K_0\|$  the maximum of the eigenvalues of  $K_0$  in Eq. (17). Here, the critical velocity for transition from Newtonian to non-Newtonian regime is  $\phi \dot{\gamma}_c \sqrt{\|K_0\|}$ .

Fig. 6a shows the evolution of  $k_n$  with  $U^*$ . As already highlighted in [29,35], the transition occurs for  $U^* \sim 1$  and all curves tend to collapse to a single one. The expression for the critical velocity is also linear in  $\dot{\gamma}_c$ . Therefore, we see that  $\dot{\gamma}_c$  only acts as a scaling parameters for the transition and that results are independent from the exact value of  $\dot{\gamma}_c$ . For  $U^* \gg 1$ , we find that  $k_n \propto (U^*)^{1-n}$ , so that the permeability follows a power-law that is identical to that of the bulk rheology of the fluid. This results was already derived theoretically [15,36] and observed experimentally [37–39] or numerically [13,14,35].

For A-type media with  $\sigma < 0.10$  and medium B, the transition occurs for values of  $U^*$  very close to one. This means that for these statistically isotropic media, the use of  $\sqrt{\|K_0\|}$  as a characteristic length in Eq. (17) provides a way to evaluate the order of magnitude of the critical average velocity associated with the transition. For highly disordered structures,  $A_1^{\sigma=0.20}$  and  $A_1^{\sigma=0.30}$ ,  $\sqrt{\|K_0\|}$  does not seem to be as accurate in predicting the transition (see magnification near the transition in Fig. 6a). We hypothesize that this is due to the anisotropy of individual realizations (see  $f$  in Table 1).  $\|K_0\|$  is indeed calculated as the maximum eigenvalue of the permeability tensor, so that  $\sqrt{\|K_0\|}$  is associated with the flow in the preferential direction (defined by the eigenvector associated to the eigenvalue  $\|K_0\|$ ). In Fig. 6a, the flow is

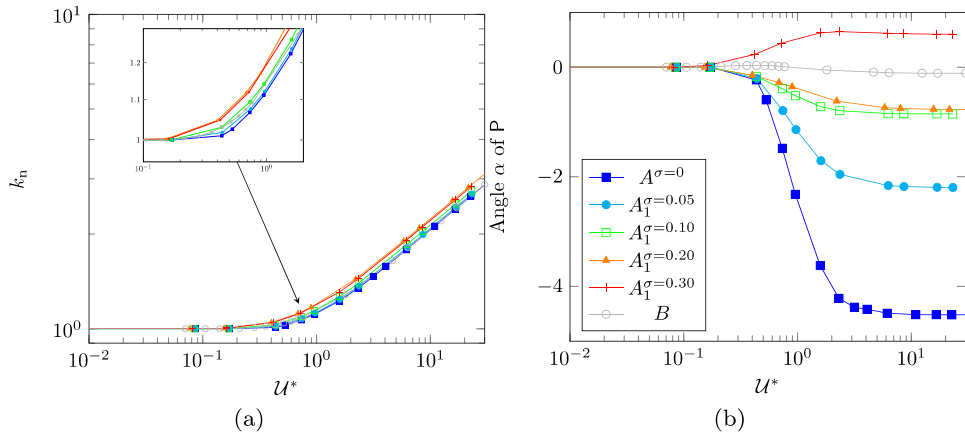


Fig. 6. Evolution of (a)  $k_n$  and (b) the angle  $\alpha$  of P plotted against the average dimensionless velocity  $U^* = \|\langle \mathbf{v} \rangle\| / (\phi \dot{\gamma}_c \sqrt{\|K_0\|})$  for several porous media. The source term direction is fixed ( $\theta = 22.5^\circ$ ) and the parameter  $n$  is set to 0.70. Same legend in (a) and (b). The inset in (a) is a magnification near the transition.

imposed at  $\theta = 22.5^\circ$ , which is not the preferential direction of media  $A_1^{\sigma=0.20}$  and  $A_1^{\sigma=0.30}$ , so that there is no reason for  $\sqrt{\|K_0\|}$  to describe accurately the transition for this flow direction.

For anisotropic media, it may therefore be interesting to use a length that is a function of the flow orientation and that differs from  $\sqrt{\|K_0\|}$ . For instance, we could diagonalize  $K_0$  to obtain the three eigenvalues and the principal axis eigenvectors. If the flow is oriented along a principal axis, we may use the square root of the associated eigenvalue as characteristic length. We could also combine the eigenvalues to calculate the lengthscale for any flow direction, which is actually what is done in reservoir simulators (see Eq. 2.83 in [40]). This new definition of  $U^*$  demands further investigations that are beyond the scope of this paper.

We then go on to study the evolution of the angles of P with  $U^*$ , an aspect of the problem that was not studied in [35,41]. For the two-dimensional A-type media, only the angle  $\alpha$  varies with  $U^*$  ( $\gamma = 0^\circ$  in Eq. (10)). For medium B, only the angle  $\alpha$  is plotted, since the angle  $\gamma$  exhibits a similar behavior. For  $U^* \ll 1$ , we observe  $\alpha = 0^\circ$  for all media, yielding an apparent Newtonian behavior ( $P = I$ ). For  $U^* > 1$ , we observe an anisotropy effect induced by the nonlinearity ( $P \neq I$ ), with a plateau reached for a fully developed non-Newtonian regime,  $U^* \gg 1$ . For  $U^* \gg 1$ ,  $\dot{\gamma}$  is higher than  $\dot{\gamma}_c$  everywhere in the liquid phase, so that the fluid behaves as a pure power-law fluid and P becomes independent from  $\|\langle \mathbf{v} \rangle\|$ . The independence of P from  $\|\langle \mathbf{v} \rangle\|$  is consistent with theoretical studies that deal with pure power-law fluids [13–15]. For medium B,  $\alpha$  and  $\gamma$  are sensitive to  $U^*$  and their evolution is not monotonous.

### 3.3. Effect of disorder on the non-Newtonian flows

We now focus on fully developed non-Newtonian flows ( $U^* \gg 1$ ) and investigate the effect of the disorder on the macroscale parameters. We study statistically isotropic media (A-type and B) in order to capture the effect of the disorder alone. For the ordered structure,  $A^{\sigma=0}$ , it is well known [13,15] that there is a significant change in the flow direction compared to the Newtonian regime, i.e.,  $\mathbf{e}_v = \frac{\langle \mathbf{v} \rangle}{\|\langle \mathbf{v} \rangle\|}$  becomes different from  $\mathbf{e}_v^0 = \frac{\langle \mathbf{v}_0 \rangle}{\|\langle \mathbf{v}_0 \rangle\|}$ . For this ordered medium, the use of a scalar correction alone in Darcy's law (Eq. (1)) is not appropriate and only a tensorial approach (Eq. 8) is accurate. However, it is unclear how disorder affects these results.

Fig. 7 shows the evolution of  $k_n^*$  (see Eq. (14)) and  $\alpha$  (see Eq. (10)) with increasing disorder. For medium  $A^{\sigma=0}$ , the standard deviation is zero,  $k_n^* = 1$  and  $E(\alpha)$  is about  $-4.5^\circ$ . For  $A^{\sigma \neq 0}$ , we observe in Fig. 7a that  $E(k_n^*)$  increases with the disorder. We also show in Fig. 7b that  $E(\alpha)$  is getting close to  $0^\circ$  as  $\sigma$  increases. This means that as disorder increases, the direction of the non-Newtonian average velocity is statistically

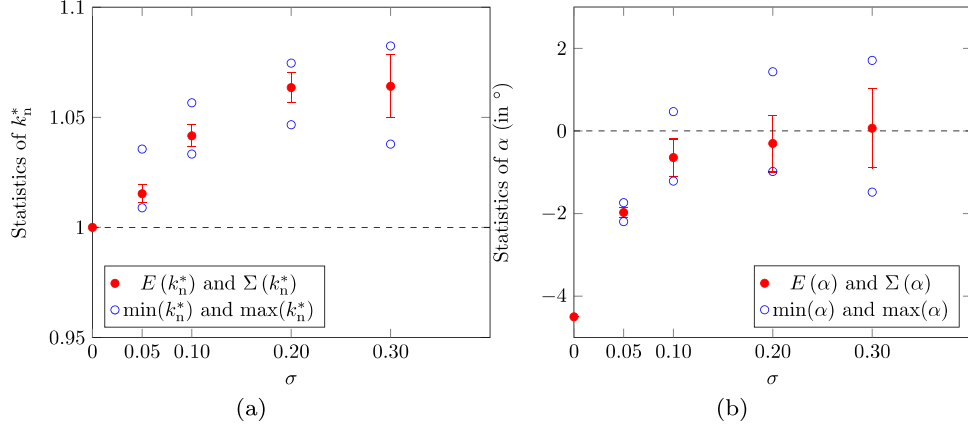


**Fig. 7.** Statistics of (a)  $k_n^*$  and (b) angle  $\alpha$  of  $P$  versus the disorder for the A-type media. The source term direction is fixed ( $\theta = 22.5^\circ$ ) and the parameter  $n$  is set to 0.70.

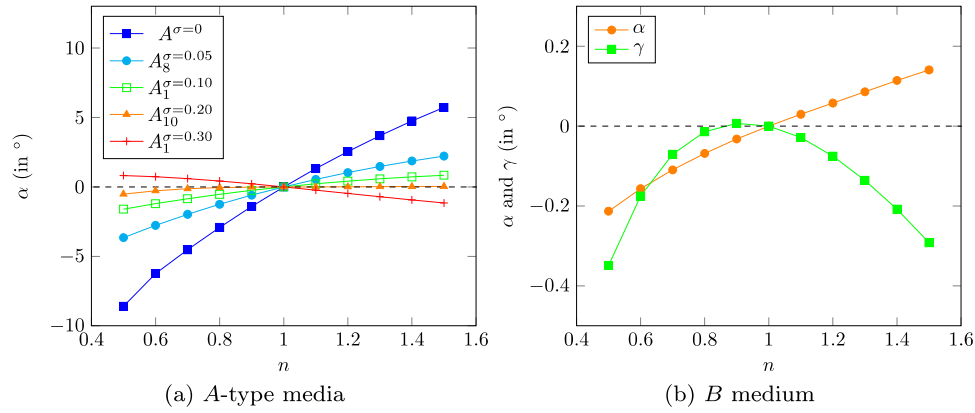


**Fig. 8.** Evolution of the angles  $\alpha$  and  $\gamma$  (associated to the rotation matrix  $P$ ) versus  $n$  for several porous media under a fully developed non-Newtonian flow ( $U^* \gg 1$ ). The source term direction is fixed ( $\theta = 22.5^\circ$ ).

getting closer to the direction of the Newtonian average velocity ( $\mathbf{e}_v \simeq \mathbf{e}_v^0$ ). In the case of the highly disordered sandstone medium  $B$ , Fig. 6b shows that, for  $U^* \gg 1$ , the angle  $\alpha$  is smaller than  $0.2^\circ$  (for the angle  $\gamma$ , the order of magnitude is the same). In the case of this sandstone, it therefore seems reasonable to consider that  $\mathbf{e}_v \simeq \mathbf{e}_v^0$ . These two results show that the effect of increasing disorder in the porous structure seems to align  $\mathbf{e}_v$  and  $\mathbf{e}_v^0$ , leading to  $P \simeq I$  and eliminating the rotation due to the nonlinear effects. This is the main result of this paper.

To go one step further, we now investigate the influence of the parameter  $n$ , which drives the nonlinearity in the PLCO rheological model. Fig. 8a shows the evolution of  $\alpha$  with  $n$  for several A-type media. For a fixed value of  $\sigma$ , the average velocity deviation increases as the nonlinearity is getting stronger, i.e.,  $|\alpha|$  increases with  $n$ . For a fixed value of  $|n - 1|$ , the average velocity deviation decreases as the disorder increases, i.e.,  $|\alpha|$  decreases with  $\sigma$ . Further, the observation that  $E(\alpha)$  gets closer to  $0^\circ$  as  $\sigma$  increases is confirmed by Fig. 8a as  $|\alpha|$  is always largest for the ordered medium. Finally, in the case of medium  $B$ , we show in Fig. 8b that the angles  $\alpha$  and  $\gamma$  remain relatively small even for large  $n$ . Here, we clearly recognize a competition between the disorder of the porous structure and the nonlinearity of the rheology. The disorder tends to weaken the influence of the rheology on the average flow orientation.

The previous results are presented for a fixed direction of the source term. Fig. 9 shows the evolution of  $k_n$  and the angles  $\alpha$  and  $\gamma$  with the source term direction, characterized by  $\theta$  (see Eq. 12), for  $U^* \gg 1$  and several porous structures. Fig. 9a and b show a  $90^\circ$  periodic and  $45^\circ$  anti-periodic behavior of  $k_n$  and  $\alpha$  for the ordered medium  $A^{\sigma=0}$ . This kind of periodic behavior has already been observed for similar 2D ordered arrays [13,15]. As expected, when the source term is imposed along a

preferential direction ( $\theta = m45^\circ$  with  $m \in \mathbb{N}$ ), the Newtonian and non-Newtonian average velocity directions are the same ( $\mathbf{e}_v = \mathbf{e}_v^0$ ) for  $A^{\sigma=0}$ .

Fig. 9 indicates that the effect of disorder also depends on the flow orientation. While the ordered medium  $A^{\sigma=0}$  exhibits a periodic behavior, this feature is weakened as the disorder increases and the magnitude of the variations of  $\alpha$  with the source term direction decreases. The same observation is true for  $k_n$  in Fig. 9a. Concerning the disordered medium  $B$ , a noisy trend is observed for  $k_n$  with  $\theta$ . The magnitude of the variations of  $k_n$  is also very small (the maximum reaches 1.3%) compared to the A-type media (for  $A^{\sigma=0}$ , the maximum reaches 11%). These observations suggest that when disorder is large enough, the sensitivity of the apparent permeability with the flow direction may be neglected.

## 4. Discussion

### 4.1. Disorder mitigates nonlinear effects

We have shown in Section 3.3 that there is a competition between the disorder of the porous structure and the nonlinearity induced by the rheology. This result is consistent with previous works in [35,42], showing that non-Newtonian effects may have little impact on the distribution of the velocity field for disordered structures. Here, using a model two-dimensional system with controlled disorder, we have extended these results to flow orientation by showing that disorder tends to limit the impact of the nonlinear rheology on the flow orientation and that the deviation angle tends to zero as disorder increases.

To gain additional physical insight into the flow direction problem, let us use a simple thought experiment. Consider a system consisting of a



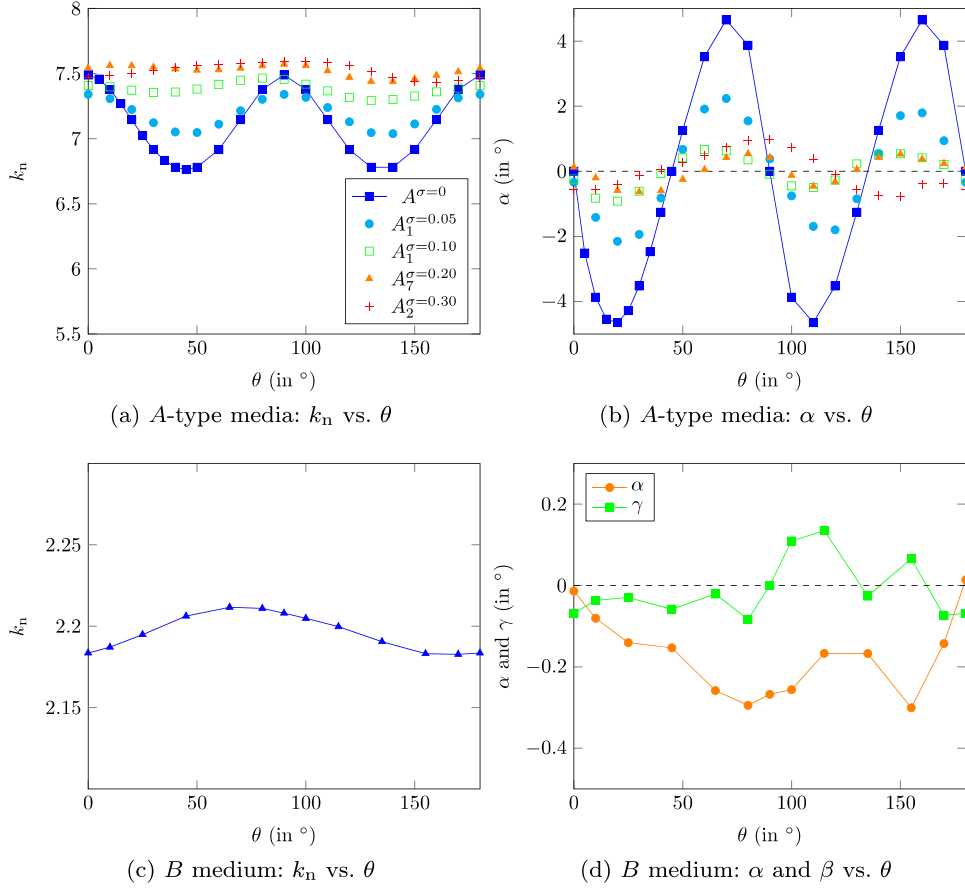


**Fig. 9.** Evolution of  $k_n$  and the angles  $\alpha$  and  $\gamma$  (associated to the rotation matrix  $P$ ) versus the source term direction (characterized by  $\theta$ , see Eq. (12)) for several porous media under a fully developed non-Newtonian flow ( $U^* \gg 1$ ). Same legend in (a) and (b). The parameter  $n$  is set at 0.70.

succession of pore bodies and pore throats. Each pore throat yields a deviation between the non-Newtonian and Newtonian flow. For instance, for  $A^{\sigma=0}$ , the deviation for each unit-cell is  $\alpha = -4.5^\circ$  between  $\mathbf{e}_v$  and  $\mathbf{e}_v^0$ . For the full domain consisting of  $15 \times 15$  unit-cells with a perfectly ordered structure, the deviation is the same,  $E(\alpha) = -4.5^\circ$ , see Fig. 7b. In this case, the effect of the rheology dominates over the disorder of the porous structure (which is zero for  $A^{\sigma=0}$ ), so that the deviation is relatively strong. However, in the case of disordered media, each pore throat tends to deviate the flow in a random direction so that, in average, the effects compensate and the deviation is small. In an infinite isotropic domain, we expect that  $\mathbf{e}_v$  would tend towards  $\mathbf{e}_v^0$  with increasing  $\sigma$ . Considering finite-size domains ( $15 \times 15$  cylinders), we observe that using ten realizations is enough to obtain  $E(\alpha) \approx 0^\circ$  for the highly disordered media  $A^{\sigma=0.30}$ . This suggests a form of ergodicity, i.e., similar behavior when averaging over space in large domains or averaging over a high number of small size realizations (see discussion in Appendix A).

For the realistic medium  $B$ , the disorder is sufficiently large to dominate over the nonlinearity, yielding small deviations of the velocity direction, i.e.  $\mathbf{e}_v \simeq \mathbf{e}_v^0$ . This suggests that models based on a scalar viscosity in Darcy's law may be accurate to account for the non-Newtonian effects in Bentheimer sandstones; although further investigations are necessary to: (1) to ensure that the angles of  $P$  remain small as the sample size increases (say  $125 \text{ mm}^3$ ) and (2) to evaluate the uncertainty and sensitivity of simulator results associated with angles of the rotation matrix  $P$  that are about  $1^\circ$ .

#### 4.2. Models used in EOR engineering

The model with the apparent viscosity is the one that is used in petroleum engineering for polymer solutions (see [40]). In these sim-

ulators, the flow is treated using an apparent viscosity in Darcy's law (see Eq. (1)),

$$\mu_{\text{app}}(\dot{\gamma}_{\text{eq}}) = \mu(\dot{\gamma}_{\text{eq}}) R_k, \quad (18)$$

where  $R_k$  is the permeability reduction factor (not necessarily constant) and  $\mu$  is the rheological law of the bulk fluid. The idea here is that the bulk fluid rheology can be used to describe the macroscale flows by introducing an equivalent shear rate,  $\dot{\gamma}_{\text{eq}}$ , which unlike the local shear rate,  $\dot{\gamma}$ , is a macroscale field. This equivalent shear rate is usually calculated as in [9] for polymer solutions

$$\dot{\gamma}_{\text{eq}} = \alpha_{\text{pm}} \frac{4\|\langle \mathbf{v} \rangle\|}{\phi R_{\text{eq}}}, \quad (19)$$

with  $\phi$  the porosity and  $\alpha_{\text{pm}}$  an empirical parameter that characterizes the impact of the porous structure and may depend on various surrounding parameters [24,39]. In Eq. (19), the norm of the average velocity is the  $L^2$ -norm. The equivalent radius  $R_{\text{eq}}$  is defined as

$$R_{\text{eq}} = \sqrt{\frac{8k_0}{\phi}}, \quad (20)$$

in the case of an isotropic medium. In the anisotropic case, a different formulation involving  $\|K_0^{-1/2} \cdot \langle \mathbf{v} \rangle\|$  is used in reservoir simulators [40]. If the medium is not isotropic, we simply use in this paper  $\|K_0\|$  instead of  $k_0$  to calculate  $R_{\text{eq}}$ , where the norm is defined as the maximum of the eigenvalues of  $K_0$ . The definitions of both  $\dot{\gamma}_{\text{eq}}$  and the equivalent radius  $R_{\text{eq}}$ , sometimes called the ‘‘pore throat radius’’, result from an analogy with the flow through a capillary tube [43].

This heuristic formulation is complex and primarily empirical. For instance, the parameter  $R_k$  takes into account the retention mechanisms

associated to the flow of polymers [40]. In practical coreflood experiments,  $R_k$  depends upon a variety of parameters, such as the salinity, concentration of polymers or even  $\dot{\gamma}_{eq}$  [44]. The dependence of  $R_k$  upon these parameters and the fundamental physics are not well understood. Further, Eq. (18) assumes that the trends of  $\mu_{app}$  and  $\mu$  are the same. Even if  $\dot{\gamma}_{eq}$  may be calibrated via the parameter  $\alpha_{pm}$  in Eq. (19), there is *a priori* no reason for the apparent and bulk fluid viscosities to be identical. In fact, in the case of PLCO fluids, this is clearly not the case.

Finally, this formulation is purely scalar and therefore is based on the assumption that the average flow direction is not modified by non-linear effects. As discussed above, the sensitivity of reservoir simulators to small perturbations in the flow direction, especially when combined with other sources of uncertainty, should be carefully assessed. Also, in oil fields, stratifications [4] or large-scale heterogeneities in the geological structure may affect this result, so that in practical situations, strong anisotropies at different scales may further complicate the matter.

## 5. Conclusions

In this work, we have investigated the flow of a model fluid with shear-dependent viscosity through porous media. In particular, we have studied the influence of the non-Newtonian effects and of the disorder of the porous structure on the apparent permeability tensor. To do so, the flow problem was solved in a variety of porous structures in order to study the behavior of the apparent permeability, which was written as  $K_{app} = k_n P \cdot K_0$  with  $K_0$  the intrinsic permeability tensor,  $P$  a rotation matrix (defined by 2 angles) and a scalar  $k_n$ . We found that there is a competition between the disorder of the porous structure and the non-linearity associated to the non-Newtonian rheology. While the nonlinearity tends to deviate the velocity direction from the Newtonian direction, disorder tends to weaken this effect. If the impact of the porous structure dominates over the nonlinearity, which seems to be the case for sandstones, a scalar correction to Darcy's law (see Eq. (18)) is sufficient. This seems to indicate that an apparent viscosity may be adapted to reservoir simulators, although further investigations are required to rigorously assess the impact of large-scale anisotropies in geological formations and the exact degree of uncertainty generated by such effects. An important extension of this work is to consider a time-dependent rheology and unsteady effects induced by flexible polymer molecules [45], such as elastic turbulence. Further, mass transport effects, retention [10] or inaccessible pore volume [46] may also significantly impact the flow orientation. From a fundamental perspective, it would also be interesting to investigate if the competition between nonlinear effects in the flow and disorder in the structure is a more general result applying to other classes of nonlinearities, such as inertial flow.

## Acknowledgments

We thank Total for the support of this study. This work was granted access to the HPC resources of CALMIP supercomputing center under the allocation p1511.

## Appendix A. Ergodicity

In Section 2.7, we have shown that considering ten A-type media of size  $15 \times 15$  cylinders was enough to obtain statistical convergence. We indeed observe a form of ergodicity between ensemble and spatial averages in Fig 4b, i.e., the variance of ensemble averaging strongly decreases with the size of the domain. To further enforce this idea, we performed simulations on a A-type medium of size  $50 \times 50$  cylinders with  $\sigma = 0.30$  (expensive calculations with about 90 million mesh elements). The size of  $50 \times 50$  was chosen because its area is approximately equivalent to 10 times the area of  $15 \times 15$  cylinders. For this large system, we found an anisotropy factor  $f = 0.97$  (see Eq. (16)). This value is very close to unity, showing that the procedure used to generate the A-type media is indeed isotropic. Further, following the framework of

Section 3.3, we also simulated a fully developed non-Newtonian flow with a source term imposed with  $\theta = 22.5^\circ$ . The resulting angle  $\alpha$  between the vectors  $\mathbf{e}_v$  and  $\mathbf{e}_v^0$  is about  $-0.1^\circ$ . This small value is very close to the average value of  $\alpha$  over the 10 A-type media at  $\sigma = 0.30$  (see Fig. 7b) which is about  $0.06^\circ$ . This proves that the results are also statistically converged for the nonlinear macroscale parameters.

## Appendix B. Volume averaging method

In this appendix, we describe the major steps of an upscaling procedure using the volume averaging method (VAM) applied to a non-Newtonian fluid for which the viscosity behavior is defined in a generic manner. Following the methodology proposed by Whitaker in [20], we show that the nonlinear problem cannot be closed in the classical manner for the Stokes linear problem. The analysis instead leads to a general non-linear relationship between filtration velocity and the gradient of the intrinsic pressure.

### Pore-scale model

We first describe the pore-scale flow model. The flow of the liquid ( $\beta$ -phase) through the rigid porous medium ( $\sigma$ -phase) is steady, incompressible and single-phase. Momentum and mass balance equations describing the flow read as follows,

$$\nabla \cdot [\mu(\dot{\gamma})(\nabla \mathbf{v} + (\nabla \mathbf{v})^T)] - \nabla p + \rho \mathbf{g} = 0 \text{ in } V_\beta, \quad (21)$$

$$\nabla \cdot \mathbf{v} = 0 \text{ in } V_\beta. \quad (22)$$

The micro-scale description contains a rheological model, expressed with a generic expression for the viscosity,  $\hat{\mu}$ , which is a function of the local shear rate  $\dot{\gamma}$ . Hence, we define,

$$\mu(\dot{\gamma}) = \mu_0 \hat{\mu}(\dot{\gamma}) \text{ in } V_\beta, \quad (23)$$

with  $\mu_0$  the Newtonian viscosity of the fluid. For the solid/liquid interface, core-flood experiments show that the Newtonian flow of polymer fluids through porous media often exhibits a permeability higher than expected. This phenomenon has been attributed to complex mechanisms between the polymer molecules and the wall, yielding an apparent slip effect [43]. Studies show that an effective slip boundary condition could describe at the pore-scale the mechanism occurring at the molecular scale [16]. Here, we will not take into account this kind of interaction and a simple no-slip condition is applied at the solid/liquid interface,

$$\mathbf{v} = 0 \text{ at } A_{\beta\sigma}. \quad (24)$$

### The framework

We consider a locally periodic porous medium. The average of a variable  $\psi$  at location  $\mathbf{x}$  is defined as

$$\langle \psi \rangle_{\mathbf{x}} = \int_{\mathbb{R}^3} m(\mathbf{x} - \mathbf{y}) \chi_\beta(\mathbf{y}) \psi(\mathbf{y}) d\mathbf{y}, \quad (25)$$

where  $\psi$  is either  $p$  or  $\mathbf{v}$ ;  $\chi_\beta$  is the fluid-phase indicator (whose value is 1 in  $V_\beta$  and 0 elsewhere); and  $m$  is a normalized kernel, i.e.,  $\int_{\mathbb{R}^3} m(\mathbf{y}) d\mathbf{y} = 1$ . The relationship between intrinsic and superficial averages is  $\langle \psi \rangle = \phi \langle \psi \rangle^\beta$ , where  $\phi = V_\beta/V$  is the porosity. Since the domain is spatially periodic, the porosity is uniform and  $\nabla \phi = 0$ .

The goal of the averaging operator is to act as a low-pass filter, yielding a well-behaved macroscale behavior. Several choices for the kernel  $m$  are available and are discussed in a series of paper from Quintard and Whitaker [27,47–50] and more recently by Davit and Quintard in [51]. In the theoretical development that follows, we assume that the kernel is correctly defined. We also decompose the flow variables as the sum of an intrinsic average and a deviation [52],

$$\psi(\mathbf{x}) = \langle \psi \rangle_{\mathbf{x}}^\beta + \tilde{\psi}(\mathbf{x}). \quad (26)$$

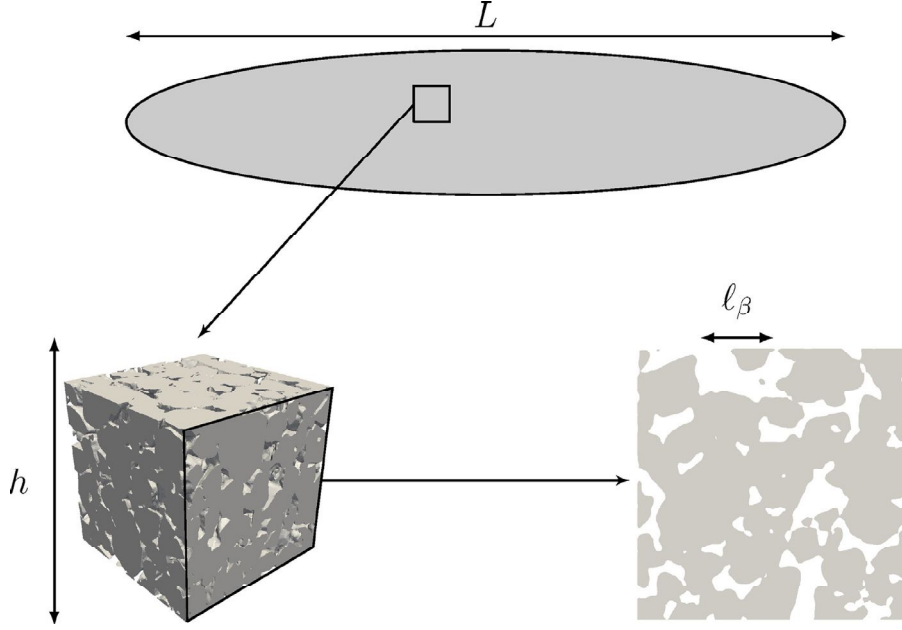


**Fig. B1.** Schematic of length-scale separation ( $l_\beta \ll h \ll L$ ). The solid phase  $\sigma$  is represented in gray.

The quantity  $\nabla \langle \psi \rangle^\beta$  reflects the variations of  $\psi$  at a large scale whereas  $\nabla \tilde{\psi}$  rather reflects micro-scale variations. The length  $l_\beta$  characterizes the micro-scale structures whereas  $L$  is associated to the macroscale domain. We assume that these length-scales are separated, i.e.,

$$l_\beta \ll h \ll L, \quad (27)$$

where  $h$  is the unit-cell size. Fig. B1 illustrates the length scale separation.

#### Averaging

We first average the mass balance equation at location  $\mathbf{x}$ . This yields

$$\langle \nabla \cdot \mathbf{v} \rangle^\beta \Big|_{\mathbf{x}} = 0. \quad (28)$$

We then average the momentum transport equation (Eq. (21)) as

$$\langle \nabla \cdot [\mu(\dot{\gamma})(\nabla \mathbf{v} + (\nabla \mathbf{v})^\top)] - \nabla \tilde{p} \rangle^\beta \Big|_{\mathbf{x}} = \nabla \langle p \rangle^\beta - \rho \mathbf{g}. \quad (29)$$

Using the spatial averaging theorem [53] along with the no-slip condition at  $A_{\beta\sigma}$  (Eq. (24)), Eq. (28) is equivalent to

$$\nabla \cdot \langle \mathbf{v} \rangle^\beta \Big|_{\mathbf{x}} = -\phi^{-1} \nabla \phi \cdot \langle \mathbf{v} \rangle^\beta \Big|_{\mathbf{x}}. \quad (30)$$

Since we assumed that the porous medium is spatially periodic, the macroscale porosity gradient is zero. This yields

$$\nabla \cdot \langle \mathbf{v} \rangle^\beta \Big|_{\mathbf{x}} = 0. \quad (31)$$

Introducing the decomposition (Eq. (26)) and the original mass balance equation in Eq. (31) leads to

$$\nabla \cdot \tilde{\mathbf{v}}(\mathbf{x}) = 0 \text{ in } V_\beta. \quad (32)$$

in which we have used the separation of scale assumption to discard gradients of  $\langle \mathbf{v} \rangle^\beta$  (the macro-scale velocity field is approximately constant over the REV). More generally, the local problem over a REV is characterized by the following approximation

$$\nabla \langle \mathbf{v} \rangle^\beta \approx 0; \quad \nabla (\langle p \rangle^\beta - \rho \mathbf{g}) \approx 0. \quad (33)$$

We also inject the decomposition into the boundary condition, which yields

$$\langle \mathbf{v} \rangle^\beta \Big|_{\mathbf{x}} = -\tilde{\mathbf{v}}(\mathbf{x}) \text{ at } A_{\beta\sigma}, \quad (34)$$

The original pore-scale momentum equation can be re-written as

$$\nabla \cdot [\mu(\dot{\gamma})(\nabla \mathbf{v} + (\nabla \mathbf{v})^\top)] - \nabla \tilde{p} - (\nabla \langle p \rangle^\beta - \rho \mathbf{g}) = 0 \quad (35)$$

to complete the governing equations for the velocity and pressure deviations.

Finally, we average the perturbation decomposition to obtain (see [51])

$$\langle \tilde{p} \rangle^\beta \Big|_{\mathbf{x}} = 0 \quad (36)$$

and

$$\langle \tilde{\mathbf{v}} \rangle^\beta \Big|_{\mathbf{x}} = 0. \quad (37)$$

#### The closure problems

In this section we analyze the solution of the coupled problems involving averages and deviations (the so-called closure).

##### The linear case

The micro-scale equations that we must solve are the continuity equation (Eq. (32)) and the momentum equation (Eq. (29)) coupled to the macro-scale equations for the averaged velocity and pressure field. For the linear case,  $p$  and  $\mathbf{v}$  may be obtained under the following form [20],

$$p(\mathbf{x}) = \langle p \rangle^\beta \Big|_{\mathbf{x}} + \underbrace{\mu_0 \mathbf{b}_0(\mathbf{x}) \cdot \langle \mathbf{v} \rangle^\beta \Big|_{\mathbf{x}}}_{\tilde{p}(\mathbf{x})}, \quad (38)$$

$$\mathbf{v}(\mathbf{x}) = \langle \mathbf{v} \rangle^\beta \Big|_{\mathbf{x}} + \underbrace{\mathbf{B}_0(\mathbf{x}) \cdot \langle \mathbf{v} \rangle^\beta \Big|_{\mathbf{x}}}_{\tilde{\mathbf{v}}(\mathbf{x})}, \quad (39)$$

in which  $\mathbf{B}_0$  and  $\mathbf{b}_0$  are closure (or mapping) variables. The problem expressed with the variables  $\mathbf{B}_0$  and  $\mathbf{b}_0$  now reads [20]

$$\Delta \mathbf{B}_0 - \nabla \mathbf{b}_0 = \langle \Delta \mathbf{B}_0 - \nabla \mathbf{b}_0 \rangle^\beta \text{ in } V_\beta, \quad (40)$$

$$\nabla \cdot \mathbf{B}_0 = 0 \text{ in } V_\beta, \quad (41)$$

$$\mathbf{B}_0 = -\mathbf{I} \text{ at } A_{\beta\sigma}, \quad (42)$$

$$\langle \mathbf{b}_0 \rangle^\beta = 0, \quad (43)$$

Periodicity of  $\mathbf{B}_0$  and  $\mathbf{b}_0$  at  $A_{\beta e}$ . (44)

with the field  $\mathbf{B}_0$  having the following property

$$\langle \mathbf{B}_0 \rangle^\beta = 0, \quad (45)$$

Then, we inject  $\mathbf{B}_0$  and  $\mathbf{b}_0$  into Eq. (29) to obtain

$$-(\nabla \langle p \rangle^\beta - \rho \mathbf{g}) + \mu_0 \langle \Delta \mathbf{B}_0 - \nabla \mathbf{b}_0 \rangle^\beta \cdot \langle \mathbf{v} \rangle^\beta = 0, \quad (46)$$

and the permeability in the classical Darcy's law reads

$$\mathbf{K}_0^{-1} = -\frac{1}{\phi} \langle \Delta \mathbf{B}_0 - \nabla \mathbf{b}_0 \rangle^\beta. \quad (47)$$

Each column of the permeability tensor  $\mathbf{K}_0$  corresponds to the Newtonian flow in response to a source term that corresponds to each unit vector of the standard basis. In this specific linear case, a solution for any vector  $\langle \mathbf{v} \rangle$  can be built by solving the three problems for  $\mathbf{B}_0 \cdot \mathbf{e}_i$  and  $\mathbf{b}_0 \cdot \mathbf{e}_i$  with  $i = 1, 2, 3$ .

#### The nonlinear case

The resolution methodology presented above relies on the superposition principle for the construction of the solution. In the nonlinear case, one has to solve the problem for  $\bar{p}$  and  $\mathbf{v}$  (or  $\bar{\mathbf{v}}$ ) (i.e., Eqs. (32), (34)–(36)) locally over a representative volume for a given value of  $(\nabla \langle p \rangle^\beta - \rho \mathbf{g})$ , which is constant over this volume thanks to the separation of scales. The resulting field can be used in the averaged momentum equation to obtain a macro-scale momentum equation under the form of a non-linear relationship between  $(\nabla \langle p \rangle^\beta - \rho \mathbf{g})$  and  $\langle \mathbf{v} \rangle$  such as

$$\langle \mathbf{v} \rangle = -\mathbf{K}_{\text{gen}} \cdot (\nabla \langle p \rangle^\beta - \rho \mathbf{g}) \quad (48)$$

where  $\mathbf{K}_{\text{gen}}$  is homogeneous to  $\text{kg}^{-1} \text{m}^3 \text{s}$  and depends on the average velocity, the rheology and the structure of the porous medium. This generic form of the macro-scale momentum equation can be put under the form of a modified Darcy's law as

$$\langle \mathbf{v} \rangle = -k_n \mathbf{P} \cdot \frac{\mathbf{K}_0}{\mu_0} \cdot (\nabla \langle p \rangle^\beta - \rho \mathbf{g}). \quad (49)$$

This formulation, according to the above development, handles the relationship between  $\langle \mathbf{v} \rangle$  and the source term  $\nabla \langle p \rangle^\beta - \rho \mathbf{g}$  with only 3 independent non-linear variables (functions of  $\langle \mathbf{v} \rangle^\beta$ , i.e., module and orientation): a scalar  $k_n$  and the angles  $\alpha$  and  $\gamma$  used in the rotation matrix  $\mathbf{P}$ . The apparent permeability tensor in Eq. (2) is therefore written as,

$$\mathbf{K}_{\text{app}}(\langle \mathbf{v} \rangle) = k_n \mathbf{P} \cdot \mathbf{K}_0. \quad (50)$$

#### References

- [1] S.G. Advani, *Flow and Rheology in Polymer Composites Manufacturing*, Elsevier Science, 1994.
- [2] J.V. Soulis, G.D. Giannoglou, Y.S. Chatzizisis, K.V. Seralidou, G.E. Parcharidis, G.E. Louridas, Non-newtonian models for molecular viscosity and wall shear stress in a 3d reconstructed human left coronary artery, *Med. Eng. Phys.* 30 (1) (2008) 9–19.
- [3] G.D. Giannoglou, J.V. Soulis, T.M. Farmakis, G.A. Giannakoulas, G.E. Parcharidis, G.E. Louridas, Wall pressure gradient in normal left coronary artery tree, *Med. Eng. Phys.* 27 (6) (2005) 455–464.
- [4] K. Sorbie, *Polymer-Improved Oil Recovery*, Springer Science & Business Media, 1991.
- [5] P. Coussot, *Rheometry of Pastes, Suspensions, and Granular Materials: Applications in Industry and Environment*, John Wiley & Sons, 2005.
- [6] R.B. Bird, P.J. Carreau, A nonlinear viscoelastic model for polymer solutions and melts, *Chem. Eng. Sci.* 23 (5) (1968) 427–434, doi:10.1016/0009-2509(68)87018-6.
- [7] A. Groisman, V. Steinberg, Elastic turbulence in a polymer solution flow, *Nature* 405 (6782) (2000) 53–55.
- [8] W. Cannella, C. Huh, R. Sright, et al., Prediction of xanthan rheology in porous media, in: *SPE Annual Technical Conference and Exhibition*, Society of Petroleum Engineers, 1988.
- [9] G. Chauveteau, Rodlike polymer solution flow through fine pores: influence of pore size on rheological behavior, *J. Rheol.* 26 (2) (1982) 111–142.
- [10] C. Huh, E. Lange, W. Cannella, et al., Polymer retention in porous media, *SPE/DOE Enhanced Oil Recovery Symposium*, Society of Petroleum Engineers, 1990.
- [11] W. Gogarty, Mobility control with polymer solutions, *Soc. Petrol. Eng. J.* 7 (2) (1967) 161–173.
- [12] J.C. Slattery, Flow of viscoelastic fluids through porous media, *AIChE J.* 13 (6) (1967) 1066–1071.
- [13] X.-H. Wang, J.-T. Jia, Z.-F. Liu, L.-D. Jin, Derivation of the darcy scale filtration equation for power-law fluids with the volume averaging method, *J. Porous Media* 17 (8) (2014) 741–750.
- [14] L. Org  as, Z. Idris, C. Geindreau, J.-F. Bloch, J.-L. Auriault, Modelling the flow of power-law fluids through anisotropic porous media at low-pore reynolds number, *Chem Eng Sci* 61 (14) (2006) 4490–4502, doi:10.1016/j.ces.2006.01.046.
- [15] Z. Idris, L. Org  as, C. Geindreau, J.-F. Bloch, J.-L. Auriault, Microstructural effects on the flow law of power-law fluids through fibrous media, *Modell. Simul. Mater. Sci. Eng.* 12 (5) (2004) 995.
- [16] F. Zami-Pierre, R. de Loubens, M. Quintard, Y. Davit, Polymer flow through porous media: numerical prediction of the contribution of slip to the apparent viscosity, *Transp. Porous Media* (2017) 1–18.
- [17] F. Garcia-Ochoa, V. Santos, J. Casas, E. Gomez, Xanthan gum: production, recovery, and properties, *Biotechnol. Adv.* 18 (7) (2000) 549–579.
- [18] Y. Davit and M. Quintard, *Handbook of Porous Media*, chapter ch. 7: Theoretical analysis of transport in porous media: Multi-Equation and Hybrid Models for a Generic Transport Problem with Non-Linear Source Terms. Taylor & Francis, 3 edition, 2015.
- [19] E. S  nchez-Palencia, *Non-homogeneous media and vibration theory*, *Non-Homogeneous Media and Vibration Theory*, 127, 1980.
- [20] S. Whitaker, Flow in porous media i: a theoretical derivation of Darcy's law, *Transp. Porous Media* 1 (1) (1986) 3–25.
- [21] H. Darcy, *Les Fontaines Publiques de la Ville de Dijon*, 1856.
- [22] M. Vakilha, M.T. Manzari, Modelling of power-law fluid flow through porous media using smoothed particle hydrodynamics, *Transp. Porous Media* 74 (3) (2008) 331–346.
- [23] L.W. Lake, R. Johns, W. Rossen, G. Pope, *Fundamentals of enhanced oil recovery*, *Soc. Petrol. Eng.*, 1986.
- [24] P. Zitha, G. Chauveteau, A. Zaitoun, Permeability dependent propagation of polyacrylamides under near-wellbore flow conditions, *SPE International Symposium on Oilfield Chemistry*, 1995.
- [25] D. Lasseux, F. Vald  s-Parada, Symmetry properties of macroscopic transport coefficients in porous media, *Phys. Fluids* 29 (4) (2017) 043303.
- [26] R. Guibert, P. Horgue, G. Debenest, M. Quintard, A comparison of various methods for the numerical evaluation of porous media permeability tensors from pore-scale geometry, *Math. Geosci.* (2015) 1–19.
- [27] M. Quintard, S. Whitaker, Transport in ordered and disordered porous media IV: computer generated porous media for three-dimensional systems, *Transp. Porous Media* 15 (1) (1994) 51–70.
- [28] L.W. Lake, *Enhanced Oil Recovery*, 1989.
- [29] F. Zami-Pierre,   coulements de solutions de polym  res en milieux poreux : lien entre physique    l'  chelle des pores et comportement macroscopique, Ph.D. thesis, Institut National Polytechnique de Toulouse, 2017.
- [30] H.G. Weller, G. Tabor, H. Jasak, C. Fureby, A tensorial approach to computational continuum mechanics using object-oriented techniques, *Comput. Phys.* 12 (6) (1998) 620–631.
- [31] S.V. Patankar, *Numerical heat transfer and fluid flow*, Series in computational methods in mechanics and thermal sciences, Hemisphere Pub. Corp. New York, Washington, 1980.
- [32] S. Roman, C. Soulaire, M.A. AlSaud, A. Kovscek, H. Tchelepi, Particle velocimetry analysis of immiscible two-phase flow in micromodels, *Adv. Water Resour.* (2015).
- [33] I. Swaid, K. Wilke, D. Kessel, Relative permeabilities and rheology of polymers in sandstone cores, *Revue de l'Institut Fran  ais du P  trole* 52 (2) (1997) 263–265.
- [34] J. Dautriat, N. Gland, J. Guelard, A. Dimanov, J.L. Raphanel, Axial and radial permeability evolutions of compressed sandstones: end effects and shear-band induced permeability anisotropy, *Pure Appl. Geophys.* 166 (5–7) (2009) 1037–1061.
- [35] F. Zami-Pierre, R. de Loubens, M. Quintard, Y. Davit, Transition in the flow of power-law fluids through isotropic porous media, *Phys. Rev. Lett.* 117 (7) (2016) 074502.
- [36] D. Getachew, W. Minkowycz, D. Poulikakos, Macroscopic equations of non-newtonian fluid flow and heat transfer, *J. Porous Media* 1 (3) (1998) 273–283.
- [37] J. Lecourtier, G. Chauveteau, Xanthan fractionation by surface exclusion chromatography, *Macromolecules* 17 (7) (1984) 1340–1343, doi:10.1021/ma00137a009.
- [38] K. Sorbie, Y. Huang, Rheological and transport effects in the flow of low-concentration xanthan solution through porous media, *J. Colloid Interface Sci.* 145 (1) (1991) 74–89, doi:10.1016/0021-9797(91)90100-M.
- [39] A. Fletcher, S. Flew, S. Lamb, T. Lund, E. Bjornestad, A. Stavland, N. Gjovikli, et al., Measurements of polysaccharide polymer properties in porous media, *SPE International Symposium on Oilfield Chemistry*, Society of Petroleum Engineers, 1991.
- [40] UTCHEM Technical Documentation, University of Texas at Austin, 2000.
- [41] F. Zami-Pierre, Y. Davit, R. de Loubens, M. Quintard, Study of the macro-scale transition emerging from non-newtonian fluid flow through porous media, in: *ECMOR XV-15th European Conference on the Mathematics of Oil Recovery*, 2016.
- [42] T. Chevalier, S. Rodts, X. Chateau, C. Chevalier, P. Coussot, Breaking of non-newtonian character in flows through a porous medium, *Phys. Rev. E* 89 (2014) 023002, doi:10.1103/PhysRevE.89.023002.
- [43] G. Chauveteau, Concentration dependence of the effective viscosity of polymer solutions in small pores with repulsive or attractive walls, *J. Colloid Interface Sci.* 100 (1984) 41–54.
- [44] D. Rousseau, I. Henaut, A. Dupas, P. Poulain, R. Tabary, J. Argillier, T. Aubry, Impact of polymer mechanical degradation on shear and extensional viscosities, *IOR 2013-From Fundamental Science to Deployment*, 2013.
- [45] A. Clarke, A.M. Howe, J. Mitchell, J. Staniland, L. Hawkes, K. Keeper, Mechanism of anomalously increased oil displacement with aqueous viscoelastic polymer solutions, *Soft Matter* 11 (18) (2015) 3536–3541.
- [46] T. L  tsch, T. Muller, G. Pusch, et al., The effect of inaccessible pore volume on polymer coreflood experiments, *SPE Oilfield and Geothermal Chemistry Symposium*, Society of Petroleum Engineers, 1985.

- [47] M. Quintard, S. Whitaker, Transport in ordered and disordered porous media i: the cellular average and the use of weighting functions, *Transp. Porous Media* 14 (2) (1994) 163–177.
- [48] M. Quintard, S. Whitaker, Transport in ordered and disordered porous media II: generalized volume averaging, *Transp Porous Media* 14 (2) (1994) 179–206.
- [49] M. Quintard, S. Whitaker, Transport in ordered and disordered porous media III: closure and comparison between theory and experiment, *Transp Porous Media* 15 (1) (1994) 31–49.
- [50] M. Quintard, S. Whitaker, Transport in ordered and disordered porous media v: geometrical results for two-dimensional systems, *Transp. Porous Media* 15 (2) (1994) 183–196.
- [51] Y. Davit, M. Quintard, Technical notes on volume averaging in porous media i: how to choose a spatial averaging operator for periodic and quasiperiodic structures, *Transp. Porous Media* 119 (3) (2017) 555–584.
- [52] S. Whitaker, The transport equations for multi-phase systems, *Chem. Eng. Sci.* 28 (1) (1973) 139–147.
- [53] F.A. Howes, S. Whitaker, The spatial averaging theorem revisited, *Chem. Eng. Sci.* 40 (8) (1985) 1387–1392.